Fuel 378 (2024) 132859

Contents lists available at ScienceDirect

Fuel

journal homepage: www.elsevier.com/locate/fuel

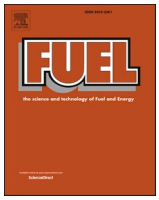

Full Length Article

Unraveling the mechanism and the role of hydrogen bonds in CO_2 capture by diluent-free amine sorbents through a combination of experimental and theoretical methods

Gabriele Manca [a,1,*], Francesco Barzagli [a,1,*], Jakub Nagy [b], Markéta Munzarová [b], Maurizio Peruzzini [a], Andrea Ienco [a]

[a] National Research Council, ICCOM Institute, via Madonna del Piano 10, 50019 Sesto F.no Florence, Italy
[b] Department of Chemistry, Faculty of Science, Masaryk University, Kotlářská 2, Brno, 611 37, Czech Republic

ARTICLE INFO

Keywords:
Carbon storage, CO_2 capture
Hydrogen bonds
Reaction mechanisms
Diluent-free sorbents

ABSTRACT

The utilization of water-lean and non-aqueous amine sorbents is regarded as an appealing approach to reduce the energy costs of CO_2 capture via liquid sorbents. However, significant research is still needed to achieve the technological maturity required for industrial-scale implementation. Here, we present a detailed experimental and computational analysis at the molecular level of CO_2 capture by dipropylamine (DPA) as a case study to deepen our understanding of the mechanisms governing CO_2 absorption by liquid secondary amines that can be used without any additional diluent. CO_2 uptake with pure DPA was investigated, and the species produced over time were determined by NMR and FT-IR spectroscopy. In particular, the NMR analysis revealed the formation of carbamic acid at high CO_2/DPA ratios. A detailed DFT investigation explained the mechanism of the reaction revealing a dynamic evolution in product distribution as CO_2 loading increases. At low CO_2 loadings, adducts with at least four DPA molecules are formed, ultimately leading to the carbamate/ammonium ionic pair stabilized through H-bonding interactions with DPA moieties. Conversely, at higher CO_2 levels some stabilizing DPA molecules of ionic pair are required for the CO_2 activation, resulting in the formation of carbamic acid. A reasonable mechanism for the evolution of product distribution is provided, and the main steps of the mechanistic picture are depicted and commented on. The dependence of carbamate and carbamic acid on the availability of hydrogen bond donors and acceptors in solution is also highlighted.

1. Introduction

The chemical capture of CO_2 from flue gases using liquid sorbents is considered a crucial technology that needs to be developed and made available as quickly as possible to limit CO_2 emissions into the atmosphere and mitigate global warming [1,2]. Aqueous solutions of alkanolamines, and particularly of monoethanolamine (MEA), are considered the most mature and suitable sorbents for large-scale industrial use, by virtue of their rapid and reversible reaction with CO_2, which ensures high capture efficiency and reusability [3–6]. However, the widespread implementation of this technique is still severely limited by the high energy costs associated with sorbent regeneration, which requires heating to temperatures between 120 and 140 °C [7–9]; for this reason, many efforts have been made in recent years to devise alternative strategies that can make the entire process less energy-intensive and industrially feasible [10,11].

An innovative strategy that has attracted the interest of several researchers is the development of water-lean and non-aqueous sorbents, which have the potential to reduce the significant regeneration energy associated with conventional aqueous sorbents [12,13]. Water has always been the most common diluent used to formulate amine sorbents, but its thermal properties, such as high heat capacity and heat of vaporization, make the regeneration of aqueous amines particularly energy intensive. Partial replacement (water-lean sorbents) or total replacement (nonaqueous sorbents) of water with organic diluents with lower thermal properties reduces the enthalpy of absorption, allowing regeneration at temperatures below 100 °C, which helps to reduce the energy required for sorbent regeneration [14,15]. Using this approach,

* Corresponding authors.
E-mail addresses: gabriele.manca@iccom.cnr.it (G. Manca), francesco.barzagli@iccom.cnr.it (F. Barzagli).
[1] Gabriele Manca and Francesco Barzagli contributed equally to this work and are the co-first authors.

https://doi.org/10.1016/j.fuel.2024.132859
Received 22 May 2024; Received in revised form 1 August 2024; Accepted 19 August 2024
Available online 25 August 2024

numerous sorbents have been formulated in recent years, including solutions of amines in alcohols or glycols, ionic liquids, biphasic solvents, CO_2-binding organic liquids (CO_2BOLs) [16–21], and their reaction mechanisms with CO_2 have been studied in detail [22–24].

Extremizing this strategy, our research group has recently considered the use of diluent-free amines: the absence of any diluent has the potential advantage of further reducing the energy cost of regeneration, since only the amine that has reacted is heated and there is no wasted energy in heating diluents (which usually account for about 70 % by weight of sorbents). In our previous studies, after a thorough screening study involving different primary, secondary and tertiary amines commonly used for CO_2 capture, we were able to identify a narrow window of compounds, all secondary amines, capable of remaining liquid both before and after CO_2 capture; these were tested in a laboratory-scale plant to assess their performance in continuous cycles of CO_2 absorption and desorption, simulating the industrial capture procedure [25,26]. As a finding, some amines, such as dipropylamine (DPA), dibutylamine (DBA), dihexylamine (DHA), and 2-(butylamino) ethanol (BAE), showed high capture efficiencies (percentage of CO_2 absorbed/CO_2 flow) during continuous absorption/desorption cycles, even when regenerated at significantly lower temperatures (75–100 °C) compared with conventional aqueous solutions [25,26]. In this regard, computational chemistry could be particularly helpful for highlighting the energetic/electronic/structural factors ruling the CO_2 absorption by amines. In recent years computational investigation at different levels of theory has been largely addressed toward aqueous solution of amines or ionic liquids for the CO_2 uptake [27–29] but few examples are available for neat amine as sorbents without any diluent.

Although we are aware that these amines cannot be directly proposed as an alternative to aqueous MEA in industrial processes, mainly due to their volatilities or viscosities, we found it interesting to further our understanding of their excellent performance through the detailed investigation at the molecular level of the different species in solution at each step of the reactivity, to gain valuable insights for the design and development of new sorbents with improved CO_2 capture performance.

For this reason, in the present work, we studied the CO_2 capture process through a combined experimental and computational approach, to unravel the reaction mechanism and to identify the nature and the relative amount of the reaction products at different CO_2 loadings. As a case study sorbent, we selected DPA, primarily due to its greater simplicity in computational analysis compared to other longer-chain or branched secondary amines. Although other research groups have previously carried out computational studies concerning CO_2 capture systems based on aqueous solutions of amines [30–32], relatively few studies have been carried out on water-lean and non-aqueous systems [22,33,34], and rare are those on CO_2 absorption directly into a solvent-free amine, which differ considerably from aqueous systems due to the different possible reactions involved. In fact, in conventional aqueous amine systems, CO_2 can be captured mainly as amine carbamate and carbonate/bicarbonate ions [4,35]. In contrast, in the absence of water or any other diluent, there are only two possible products resulting from the straightforward CO_2 capture by amines, namely (i) the ion pair formed by carbamate and protonated amine, and (ii) the carbamic acid [23–26].

In the present experimental study, the uptake of CO_2 by pure DPA, without the addition of any diluent, was evaluated at a temperature of 20 °C in terms of CO_2 loading, as measured by the gradual increase in solution weight. The qualitative and quantitative variation of the different products in solution over time (as the CO_2 loading increased) was thoroughly evaluated by means of an accurate speciation study using ^{1}H and ^{13}C NMR spectroscopy, a powerful analytical technique that can provide valuable information for understanding the reaction mechanisms and interactions between different species [23,36]. In addition, the evolution of the different species in solution was further investigated by FT-IR analysis, and a possible reaction mechanism based on stabilization of carbamic acid by hydrogen bonding with the carbamate was proposed. The obtained results were then validated and explained by Density Functional Theory (DFT) investigation, which not only identified all the potential species originated by CO_2 activation for different CO_2 loadings but also provided reasonable energetic pathways for their formation and interconversion. Also, hydrogen bonding provided by free DPA was found to have a pivotal role in the stabilization of carbamate. This multifaceted approach sheds light on the mechanism responsible for the CO_2 capture performance of DPA and similar amines, and suggests insights for the development of more efficient and environmentally friendly sorbents for carbon capture technologies.

2. Experimental section

2.1. CO_2 absorption experiments

The secondary amine dipropylamine (DPA, > 99 %) was purchased from Sigma-Aldrich and used as received without further purification. Pure CO_2 (99.9999 %) was obtained from Rivoira Srl.

CO_2 absorption by DPA without diluents was studied experimentally according to a previously validated procedure [37]. In this, the absorber (a Drechsel gas washing bottle with a sintered glass diffuser with 16–40 μm pores) was charged with 35.0 g of DPA (0.346 mol) and weighed, to record the initial weight. Subsequently, the absorber was immersed in a thermostatted bath (Thermo Scientific AC200-A25) to ensure a constant temperature of 20 °C and was fed with pure CO_2 at a constant flow rate of 0.370 molCO_2 h^{-1}, controlled by a gas flow meter (Cole Parmer). A cold condenser, kept at −5 °C, was used to avoid amine loss during absorption. The experiment was divided into five consecutive time steps, namely: step-1 between 0 and 5 min; step-2 between 5 and 10 min; step-3 between 10 and 30 min; step-4 between 30 and 60 min; and step-5 between 60 and 90 min. At the end of each step, the CO_2 flow was temporarily interrupted: the absorber was weighed, and a small sample of the solution (DPA+formed products) was taken for NMR and FT-IR analysis. The absorber was then weighed again, and the CO_2 supply was resumed. The difference between the weight recorded at the end and beginning of each step provided the weight increment, *i.e.* the amount of CO_2 (g) captured, and consequently, the increase in CO_2 moles absorbed (Δabs). Absorption was stopped definitively after 90 min. The CO_2 loading (α), *i.e.*, the ratio between the amount of CO_2 absorbed and the total amine (mol CO_2 captured/mol DPA), was calculated at each step of the absorption using the following equation, where Δabs_i represent the mol of CO_2 absorbed in the step *i.*:

$$\alpha_i = \frac{\sum_{i=1}^{5} \Delta abs_i}{molDPA}$$

2.2. NMR and FT-IR analysis methods

^{1}H NMR and ^{13}C NMR spectra were recorded at each absorption step, namely after 5, 10, 30, 60 and 90 min, using a Bruker Avance III 400 spectrometer operating at 100.613 MHz at a temperature of 20 °C. Sample preparation method, NMR instrumental parameters and analysis procedure were the same as those used and validated in our previous works [38,39]. In the ^{13}C NMR spectra (or, more correctly, ^{13}C{^{1}H}, since the spectra were acquired with proton decupling) the homologous carbon atoms of the DPA and protonated DPA ($DPAH^+$) species exchange rapidly on the NMR scale via proton scrambling, giving a unique signal. The same occurs between carbamate and carbamic acid. The peaks integration of the carbon atoms of the $–CH_2–$ and $–CH_3$ backbone of the DPA allowed us to calculate the relative percentages of the sum of carbamate + carbamic acid and the sum of DPA+$DPAH^+$. Taking a single carbon atom as a reference, the amount (mol) of CO_2 absorbed can be estimated (error < 2 %) using the following equation:

$$CO_2abs = Am_0 * \frac{S_c}{S_c + S_a}$$

where Am_0 is the initial amount (mol) of DPA, S_c is the subtended area of the carbamate + carbamic acid peak, and S_a is the subtended area of the DPA+DPAH$^+$ peak. Although DPA and DPAH$^+$ provide a unique signal, their relative amounts can be assessed from the chemical shift (δ, ppm) of their signals after constructing appropriate calibration lines. The limit values found for each carbon atom of free amine were: [δ(–***C***H$_3$) = 11.72 ppm; δ(C–***C***H$_2$–C) = 23.74 ppm; δ(C–***C***H$_2$–N) = 52.24 ppm], while for fully protonated DPAH$^+$ (obtained with the addiction of an excess of HCl) were: [δ(–***C***H$_3$) = 110.90 ppm; δ(C–***C***H$_2$–C) = 19.37 ppm; δ(C–***C***H$_2$–N) = 49.45 ppm]. Finally, it is possible to obtain an estimate of the amount of carbamic acid present in solution: in fact, given the amount of protonated amine, it can be assumed that the DPA carbamate species must be in the same amount to ensure the neutrality of the solution. Consequently, the amount of carbamic acid can be calculated by subtracting the amount of DPAH$^+$ from the value found as the sum of carbamate + carbamic acid.

In addition, Fourier transform infrared (FT-IR) spectra of DPA at the beginning of the experiment (pure amine) and during absorption were recorded with a PerkinElmer Spectrum BX FT-IR System, using a KBr disk, in the 4000——400 cm^{-1} range with a resolution of 2 cm^{-1}.

2.3. Computational details

All the intermediates and Transition States were optimized at DFT-B97D [40] level of theory within the Gaussian16 package [41], using the CPCM model [42] for the DPA experimental solvent. Triple Zeta basis set TZVP [43] was used for all the atomic species. The functional was chosen to include the dispersion forces for better considering the weak intermolecular interactions between the species in solution. All the optimized structures were validated as minima and/or transition states by computed vibrational frequencies. Cartesian coordinates and energetic features of all the optimized structures are reported in the Supporting Information.

3. Results and discussion

3.1. CO_2 absorption and speciation investigation

As reported in a previous study,[25] DPA can efficiently capture CO_2 contained in a gaseous mixture without the need for any diluent: in fact, this secondary amine remains liquid before and after CO_2 absorption. In this study, the absorption of CO_2 by this solvent-free amine was evaluated by measuring the weight increase of an absorber, containing 35.0 g of DPA, which was fed with pure CO_2 at a flow rate of 0.370 molCO_2 h^{-1}, as described in Section 2.1. From the weight increase, the amount CO_2 absorbed (at a given time) was calculated, and consequently the loading, *i.e.* the ratio between the captured CO_2 and the amount of amine. The loading values obtained from weighing during the CO_2 absorption experiment are shown in Table 1.

CO_2 loading increases rapidly in the first 30 min (up to loading = 0.491), then the increase is progressively slower. After 90 min of absorption, the loading (by weight) was 0.645. By further prolonging the CO_2 capture, the loading increases only slightly, reaching a value of 0.662 after a total of 285 min. As evident, this loading value is significantly higher than the theoretical value of 0.5 expected from conventional 2:1 stoichiometry between amine and CO_2, and the difference cannot be explained by physical absorption alone [44,45]. Actually, in the absence of water, and any other organic diluent capable of interacting with CO_2 when an alkaline species is present, DPA [$(CH_3CH_2CH_2)_2NH$] can react with CO_2 to form the ion pair protonated DPA/DPA carbamate $[(CH_3CH_2CH_2)_2NH_2]^+[(CH_3CH_2CH_2)_2NCO_2]^-$ (reaction 1, stoichiometric ratio DPA:CO_2 = 2:1), or the corresponding DPA carbamic acid [$(CH_3CH_2CH_2)_2NCOOH$] (reaction 2, stoichiometric ratio DPA:CO_2 = 1:1) [25,44].

2 $(CH_3CH_2CH_2)_2NH+CO_2 \rightleftarrows [(CH_3CH_2CH_2)_2NH_2]^+[(CH_3CH_2CH_2)_2NCO_2]^-$ (1).

$(CH_3CH_2CH_2)_2NH+CO_2 \rightleftarrows (CH_3CH_2CH_2)_2NCOOH$ (2).

In order to unravel the mechanism of the reaction between DPA and CO_2, a speciation study was carried out during CO_2 uptake: small aliquots of amine were taken at successive times of uptake, and specifically after 5, 10, 30, 60 and 90 min. The samples were analyzed by ^{1}H NMR and ^{13}C NMR to determine the species qualitatively and quantitatively in solution as the reaction proceeded, following the procedure described in Section 2.2. Fig. 1 shows how the speciation of the absorbent solution varies as CO_2 capture proceeds. The complete recorded ^{1}H NMR and ^{13}C NMR spectra are shown in Figures S1 and S2 in the Supporting Information.

Generally, both aqueous and non-aqueous solutions of secondary amines react with CO_2 to form carbamate: the formation of carbamate is kinetically favored over other possible products (bicarbonate or alkyl carbonates, depending on whether water or organic diluents are used) [35]. Even in the case of DPA, although in the absence of any solvent, the first product formed is carbamate (reaction 1). Looking at the ^{13}C NMR spectra in Fig. 1, it is clear that the signals associated with carbamate increase as loading increases: in particular, consistent with the loading values obtained by weighing, carbamate is present in small amounts at the beginning (α = 0.161), has about the same intensity as the DPA/DPAH$^+$ signals at α = 0.492, and becomes the most abundant species at the end of the capture process (α = 0.631).

Unlike what usually happens when the amine is in solution, however, in this case the signals associated with the carbamate shift to higher fields (lower ppm values) as absorption proceeds: this may indicate the presence of another product, carbamic acid (via reaction 2), which provides the same ^{13}C NMR signals as the carbamate. As a matter of fact, the carbamate and carbamic acid species are in rapid equilibrium via proton scrambling: their unique signal (marked with an asterisk, in Fig. 1) shifts during the capture process, indicating that one product grows more than the other one during the process. Looking also at the ^{1}H NMR spectra, at α = 0.492 a new signal (h*) appears in the range 10–11 ppm, which was not present before. This signal is attributable to the proton of carbamic acid, in fast exchange with the carbamate ion (and moves to higher ppm values as the carbamic acid increases) [23]. It follows that, as CO_2 capture proceeds, the amount of carbamic acid increases at the expense of carbamate, thus justifying loading values greater than 0.5 (which would be the maximum obtainable if capture occurred only by reaction 1). Similarly, as the amount of CO_2 absorbed increases, the relative amount of DPAH$^+$ to DPA increases: these two species provide a single signal, which shifts to higher fields (lower ppm values) as DPAH$^+$ increases. Similar ^{1}H and ^{13}C NMR speciation results were also obtained by Kortunov *et al.* for primary amines in organic diluents [23].

The amounts (mol) of all species present at the different absorption steps, as well as the resulting CO_2 loading, calculated by ^{13}C NMR according to the procedure described in Section 2.2, are given in Table 1. As a first result, the CO_2 loading values calculated by ^{13}C NMR are in excellent agreement with those obtained by weighing, with variations in the order of 0.2–6 %, underlining the reliability of this method, and the

Table 1
CO_2 loading (mol CO_2/mol DPA) as a function of uptake time, measured by weighing, and CO_2 loading and amount (mol) of species in solution as a function of uptake time, determined by ^{13}C NMR analysis.

Time (min)	Loading by weight	Loading by NMR	DPA (mol)	DPAH$^+$ (mol)	Carbamate (mol)	Carbamic acid (mol)
0	0	0	0.346	0	0	0
5	0.089	0.085	0.289	0.028	0.028	0.001
10	0.173	0.161	0.242	0.049	0.049	0.007
30	0.491	0.492	0.060	0.116	0.116	0.054
60	0.609	0.599	0.019	0.120	0.120	0.087
90	0.645	0.631	0.012	0.116	0.116	0.103
285	0.662					

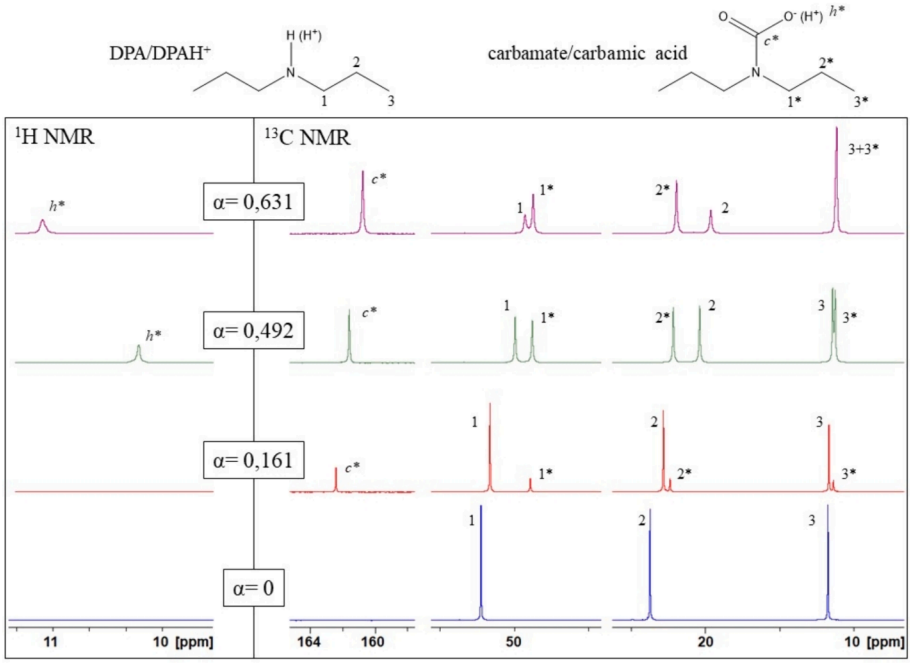

Fig. 1. ^{1}H NMR and ^{13}C NMR spectra of DPA as a function of the increasing CO_2 loading (α) during absorption experiments with pure CO_2 at T=20 °C. The height of the peaks at 160–164 ppm in the ^{13}C NMR spectra is not in scale. The reported loading values are those calculated by ^{13}C NMR.

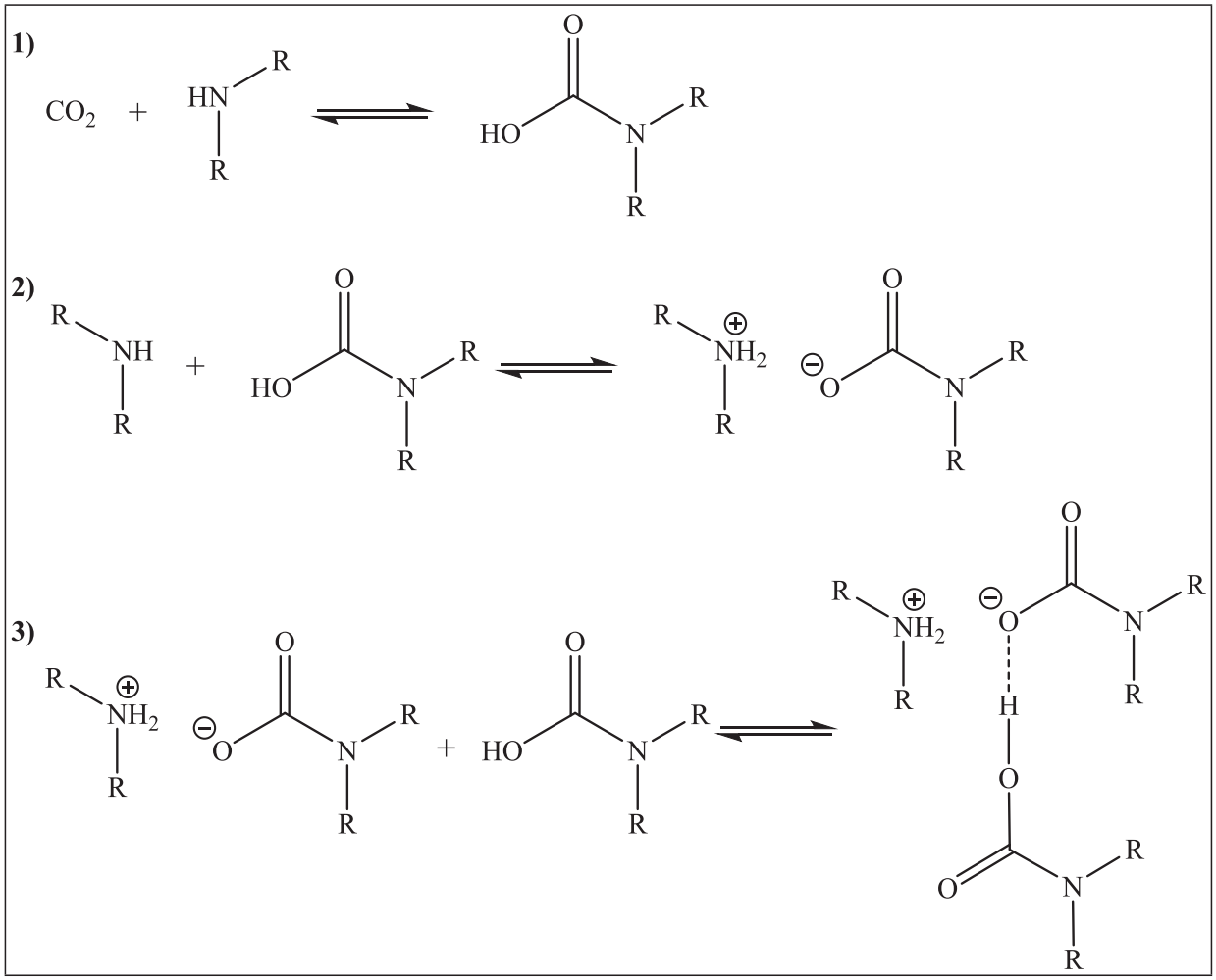

Scheme 1. Series of equilibria proposed to describe the CO_2 capture process with solvent-free DPA (R=–$CH_2CH_2CH_3$).

negligible impact of volatilization under these particular experimental conditions; furthermore, the difference found for prolonged absorption can be attributed to a small physical absorption. Analyzing the quantities calculated for the different species, it can be seen that at the beginning of the reaction (5—10 min), the captured CO_2 is converted almost entirely to carbamate; subsequently (over 30 min), the amount of carbamate remains almost unchanged, while the amount of carbamic acid increases significantly until it reaches values very close to that of carbamate (at 90 min). These values show that, under our operating conditions, CO_2 is almost entirely absorbed as carbamic acid after 30 min. It is also interesting to note that, between 60 and 90 min, the loading increases, the carbamic acid increases, while the amount of carbamate decreases suggesting a direct correlation between these two species in solution.

These data suggest a possible reaction mechanism based on the stabilization of carbamic acid by hydrogen bonding with the carbamate (Scheme 1), similar to that proposed by Switzer *et al.* in their studies on ionic liquids capable of stabilizing carbamic acids [44].

The first reaction shown in Scheme 1 relates to the formation of carbamic acid from DPA and CO_2, with a stoichiometric ratio of 1:1. In the absence of water or other diluents, free dipropylamine is both the reactant and the solvent of the reaction: given the large amount of free DPA available at the beginning of the experiment, the carbamic acid formed is readily deprotonated by the surrounding alkaline environment, obtaining the conventional $DPAH^+$/DPA-carbamate ion pairs, as shown in the second equilibrium. As CO_2 absorption continues, the amount of free DPA available becomes progressively smaller, while the amounts of $DPAH^+$ and carbamate continue to increase (Table 1): as a matter of fact, the free amine is no longer the reaction solvent, but is replaced by the increasing amount of the ionic pair. In this particular condition, as shown by the third equilibrium proposed in Scheme 1, the carbamic acid formed can be stabilized through hydrogen bonding with the carbamate anion.

It is worth emphasizing that in the process proposed in Scheme 1, the stoichiometric ratio between DPA and CO_2 is 3:2. This stoichiometry would give a theoretical maximum CO_2 loading of 0.667, which is in excellent agreement with the value obtained by weighing after 285 min (Table 1) and with the loading values reported for absorptions conducted with similar solvent-free secondary amines [25].

Further evidence for the formation of both carbamate and carbamic acid comes from FT-IR analysis, conducted on DPA before, during and at the end of CO_2 absorption. The spectra obtained are shown in Fig. 2. As clear from the comparison with the spectrum of pure DPA ($\alpha = 0$), after 10 min of absorption ($\alpha = 0.161$), the formation of characteristic signals of the $DPAH^+$/carbamate ion pair can be observed, in particular the asymmetric COO^- stretching of carbamate (1547 cm^{-1}), the C-O bond (1265 cm^{-1}) and the NH_2^+ signals of the secondary ammonium ion at 2552, 1621 and 1411 cm^{-1} [46–49]. After 90 min of absorption ($\alpha = 0.631$), the signals correlated with carbamic acid are also evident. In fact, the appearance of the new signal at 1680 cm^{-1} related to the carbonyl of carbamic acid [25,44,46,49] is accompanied by a significant broadening of the band at 2600–3100 cm^{-1}. The latter band, generally assigned to the dissolved CO_2, also includes the O–H carbamic acid stretching as already reported in literature [44,49]. To have a complete overview of all the potential species in solution as well as of their formation, a DFT analysis was carried out considering the variable CO_2/DPA ratios.

3.2. Computational investigation

3.2.1. Low CO_2 loadings (lower CO_2/DPA ratio)

The first step of the computational investigation concerns the formation of the initial adduct between CO_2 and the amine. Many articles related to the CO_2 activation by amines have highlighted the requirement of at least two molecules of amine involved in the process [50]. In this specific case, the optimization of a 1:1 DPA/CO_2 adduct provides a minimum structure featuring a large N(DPA)—C(CO_2) distance of 2.82 Å with a still inactivated CO_2 molecule showing the linear O-C-O arrangement. The result suggests a too weak nucleophilic character of the nitrogen to allow the activation of the CO_2. Being the DPA the solvent, in the absence of any other species in solution, the H-bonding between two amine moieties could favor the CO_2 activation since by weakening the N–H linkage, the basicity of the amine could be improved. In this regard, the optimized structure of a first adduct [$(DPA)_2$*(CO_2)], **1**, shown in Fig. 3, features an already activated CO_2 moiety being O1C1O2 angle of 144° and a N1—C1 distance of 1.86 Å, one Ångström shorter compared with the adduct involving a single DPA molecule. The bent CO_2 structure in the calculated initial adduct **1** is confirmed by the computational detection of an IR peak at 1855 cm^{-1} for the C=O stretching, suggesting the occurrence of electron transfer from amine to CO_2. The latter acquires a total net Mulliken charge [51] of −0.4 (mainly localized on the oxygen centers) in **1** compared to the starting neutral one in the isolated molecule. The obtained adduct could be reasonably described as a zwitterionic species with the initial formation of a N1—C1 bonding with the nitrogen center featuring a tetrahedral arrangement with a less electron-rich nitrogen in favor of the oxygen atoms.

A further stabilization of the adduct may result from the involvement of additional amine molecules in hydrogen bonding with the oxygen atoms of the activated CO_2, as reasonably occurs at low CO_2 loadings. Given the dual role played by DPA, both as an absorbing species and as a diluent, several adducts with increasing CO_2/DPA ratios from 1/6 to 1/3 were computationally studied, mimicking the experimental increase in the CO_2/DPA ratio during the absorption process. In all cases, CO_2 was

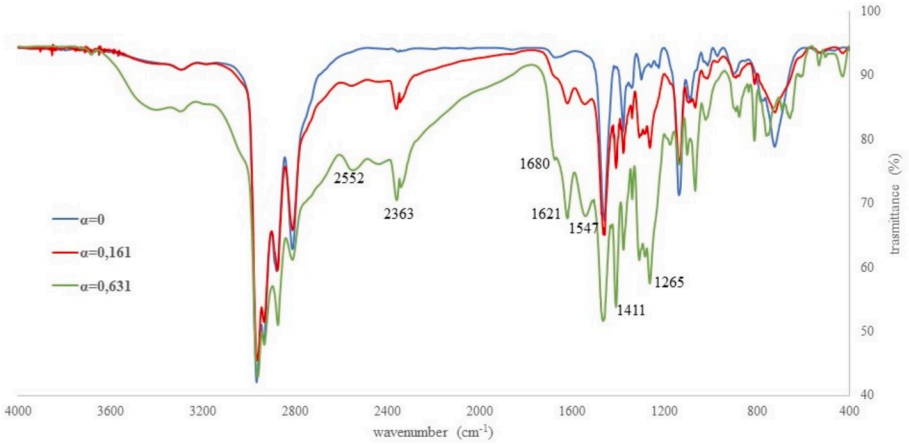

Fig. 2. FT-IR spectra of DPA at different CO_2 loading (α).

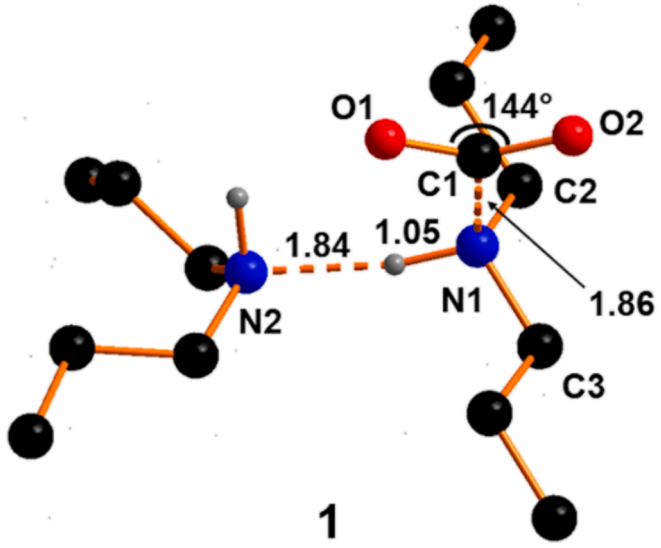

Fig. 3. Optimized structure of the adduct [$(DPA)_2$*CO_2], **1**. For the sake of clarity only the protons involved in H-bonding interactions have been shown.

already activated and no particular influence was found within a range of CO_2/DPA ratios between 1/6 and 1/4. Thus, the computational analysis focused mainly on the evolution of two adducts of **1** with one or two further DPA molecule(s). The first adduct involving three DPA molecules, namely [$(DPA)_3$*(CO_2)], is shown in Figure S3 in Supporting Information, while the second one [$(DPA)_4$*(CO_2)], adduct **2**, is shown in Fig. 4. The involvement of a larger number of DPA molecules allows a stepwise shortening of the N1—C1 distance, up to 1.70 Å in **2,** suggesting a more efficient electron donation from amine to CO_2, as confirmed by the closure of the OCO angle. The bent structure of CO_2 is mirrored by the appearance of a calculated IR active stretching mode at 1754 cm^{-1} for **2**, possibly due to the synergic action of the hydrogen bonding between the aminic proton and oxygen atoms and the DPA nitrogen → CO_2 electron donation. The evolution of the frontier molecular orbitals of the CO_2 upon bending is shown in Scheme 2. The *in-plane* LUMO is stabilized in energy and the contribution of the central carbon atom is increased, while the *out-of-plane* orbital is only slightly influenced by geometrical perturbation. A similar behavior is found for the *in-plane* and *out-of-plane* HOMOs. CO_2 activation should be favored by a combined nucleophilic attack on the central carbon and electrophilic interactions on the oxygen atoms [52–54]. From the perspective of the various adducts computationally addressed, the greater is the number of DPA molecules involved, the more efficient become the hydrogen-bonding interactions in stabilizing the starting adducts. An

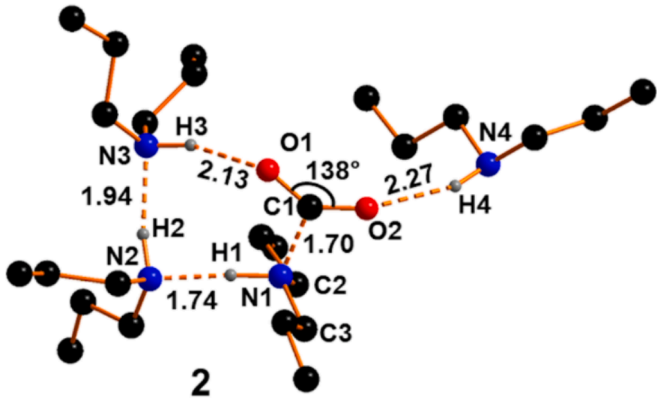

Fig. 4. Optimized structure of the adduct **2**. For the sake of clarity only the protons involved in H-bonding interactions have been shown.

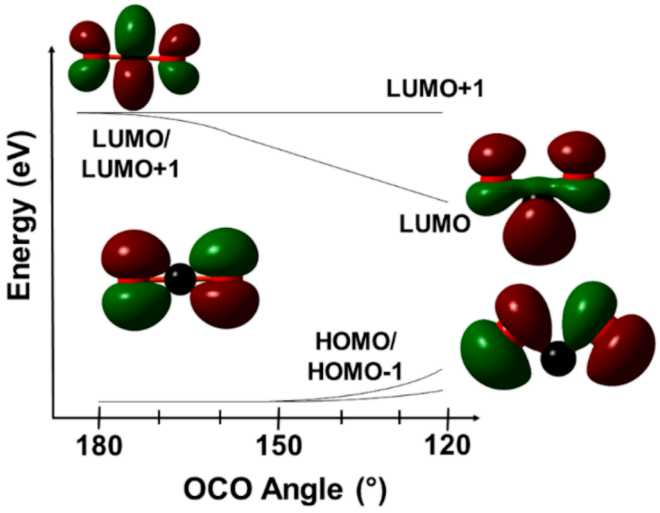

Scheme 2. Energetic evolution of the frontier molecular orbitals of CO_2 upon tightening the OCO angle (from 180° to 120°).

efficient nitrogen donation toward the carbon center of CO_2 stabilizes the LUMO, and the more available electron density on CO_2 unit allows its localization on the lateral oxygen atoms, thus a more pronounced ability for H-bonding pattern.

In recent years, the bifunctional CO_2 activation, even without metal assistance, has become a very popular topic in developing new sustainable and efficient ways for CO_2 capture and valorization [55–59]. The bifunctional systems require the synergistic action between electrophilic and nucleophilic species, where the former (generally transition metals, salts or protons involved in hydrogen bonding) have the role of immobilizing and, in some way, asymmetrizing the CO_2 through interaction with the oxygen, while the latter (amines, epoxides) act as electron donors toward the carbon center. In the present case, the bifunctional system is made up by the N–H protons as electrophiles and by the nitrogen atoms as nucleophiles, so the solvent plays the double role of nucleophile and electrophile. In all the optimized starting adducts the bonding between N1 and C1 is still far from being comparable with that in carbamic acid or carbamate anion, being the N1-C1 distance invariably long (1.70–1.86 Å) and the dihedral angle C3N1C1O1 close to 60°. The optimized structure of an isolated carbamate or a carbamic acid features N1-C1 distance between 1.36 and 1.44 Å and a planar configuration around nitrogen center with C3N1C1O1 dihedral angle not larger than 10°. The adduct **2** should evolve toward the final achievement of a partial double N1-C1 bond and for the detailed analysis of the mechanism the adduct **2** with four DPA molecules was used as a model of the experimental conditions with low CO_2 loadings with respect to the amine.

The first reasonable step toward the formation of the carbamic acid or carbamate could be the H1 transfer from N1 to N2 providing an intermediate ionic pair with the carbamate at N1 and the ammonium counterion (the protonated DPA) at N2. A relaxed scan associated with the shortening of the H1-N2 distance highlights the presence of a Transition State, namely $\mathbf{TS_{2\text{-}3}}$ shown in Fig. 5, featuring the H1 center halfway between N1 and N2 being the N1-H1 and N2-H1 distances 1.37 and 1.25 Å, respectively. As shown in Fig. 5, the proton transfer increases the nucleophilicity of N1 center toward CO_2 with a shortening of the N1-C1 distance of around 0.12 Å and an O1C1O2 angle closure by 5.0° respect **2**. The free energy barrier for the achievement of the Transition State $\mathbf{TS_{2\text{-}3}}$ has been estimated to be as small as 3.5 kcal mol^{-1} with an associated single imaginary frequency at −781 cm^{-1} showing the proton exchange between N1 and N2. After $\mathbf{TS_{2\text{-}3}}$, the system evolves toward a minimum structure **3**, shown in Figure S4 in Supporting Information, for the final formation of the N2-H1 bonding with a free

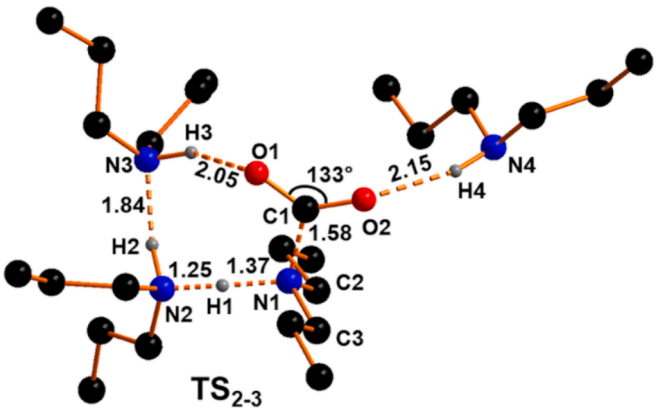

Fig. 5. Optimized structure of the Transition State **TS_{2-3}**. For the sake of clarity only the protons involved in H-bonding interactions have been shown.

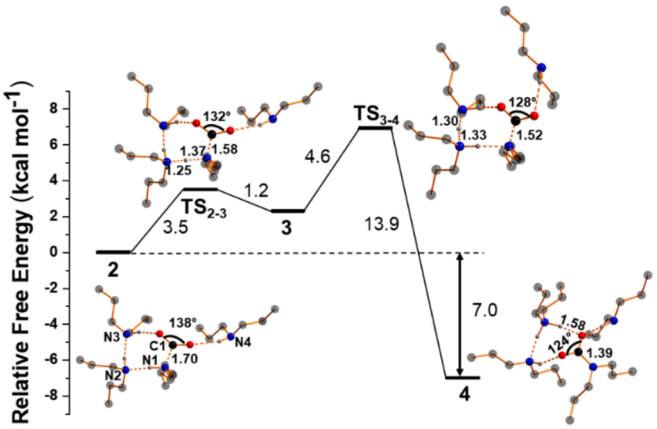

Fig. 7. Free energy (kcal/mol) reaction pathway from **2** to **4**.

energy gain as small as −1.2 kcal mol^{-1}. As obtained for the starting adduct, the dihedral angle C3N1C1O1 (35°) is still far from the final value of the carbamic acid or carbamate anion.

The final ionic pair **4** (see Fig. 6) featuring the real carbamate anion and ammonium cation is achieved through a second proton transfer, the H2 from N2 to N3, by the Transition State **TS_{3-4}** with an associated free energy barrier of + 4.6 kcal mol^{-1} and an imaginary frequency at −920 cm^{-1}. In **TS_{3-4}**, shown in Figure S5 in Supporting Information, the obtained dihedral angle C3N1C1O1 is approximately 27°. The final minimum **4**, shown in Fig. 6, features a rotated O1C1O2 moiety with a dihedral angle C3N1C1O1 of 5° *ca.* with a free energy gain of −13.9 kcal mol^{-1} compared to **TS_{3-4}** and of −7.0 kcal mol^{-1} compared to the starting adduct **2**. The calculated IR spectrum satisfactorily compares with the experimental one obtained for α = 0.161. In particular, the COO stretching mode is obtained at 1511 cm^{-1}, the diagnostic peaks for the N–H stretching of the ammonium cation are found at 1696 and in between 2332 and 2553 cm^{-1}. The O-C-N stretching of the carbamate is detected in the region of 1252 and 1261 cm^{-1} coupled with other molecular modes.

A schematic free energy profile for the obtainment of **4** starting from adduct **2** is shown in Fig. 7. From a structural viewpoint along the reaction pathway from adduct **2** to **4**, the angles of the very-weak initial H-bonding interactions between CO_2 oxygen atoms and the DPAs (N–H-O angle of ca. 160°) become wider up to the final value of 171°, highlighting the strengthening of the interaction, as also evidenced by the shortening of the H-bonding distances. A detailed list of all the distances and angles involved in the hydrogen bonding interaction in all the optimized intermediates, Transition States and products can be found in Table S1 in Supporting Information.

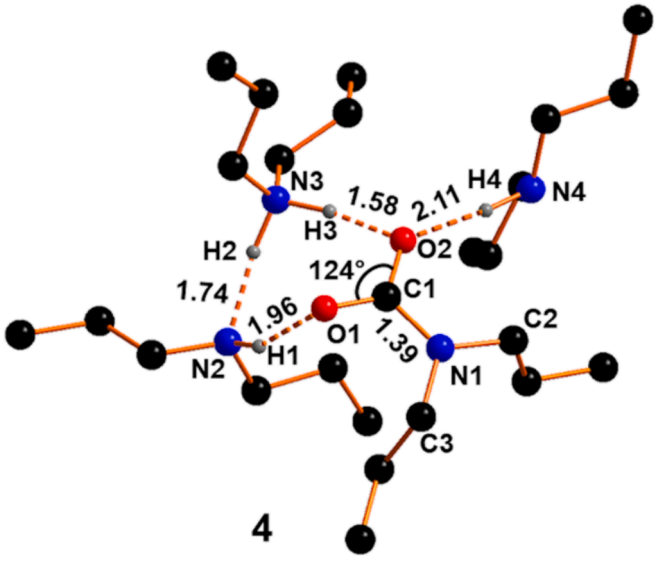

Fig. 6. Optimized structure of the ionic pair **4** stabilized by DPA molecules. For the sake of clarity only the protons involved in H-bonding interactions have been shown.

In conclusion, at low CO_2 loadings adducts of type **2** are plausible in DPA and the ionic pair is then obtained through a double proton transfer coupled with a rotation of the activated CO_2 around the C-N bonding. All the efforts to optimize an isomeric form of the adduct **4**, featuring a carbamic acid stabilized by three DPA molecules failed, once again excluding the carbamic acid formation at least at low CO_2 loading. Similar results have invariably been obtained also for a 1:3 up to 1:6 CO_2/DPA ratios. A complete free energy pathway for the reactivity of the adduct [$(DPA)_3$*(CO_2)] toward the formation of the ionic pair is reported in Figure S6 in Supporting Information.

3.2.2. *High CO_2 loading (higher CO_2/DPA ratio)*

The previous section has highlighted the importance of DPA molecules for stabilizing the ionic pair carbamate/ammonium, as shown in adduct **4** in Fig. 6. The experimental tests have revealed that by increasing the CO_2 loadings the carbamic acid is formed, as detected by ^{1}H NMR spectra, with the appearance of a new peak in the 10–11 ppm range, reasonably assigned to the carbamic acid proton (*h**) and not detected previously at lower α values. In addition, the IR investigation revealed a broadening of the band 2600–3100 cm^{-1}, generally assigned to the dissolved CO_2, due to the appearance of new peak for O–H stretching of carbamic acid. The more availability of CO_2 requires that some DPA molecules, originally (low CO_2 loading) involved in the formation of an adduct like **4**, should be involved in the activation of CO_2. To simulate the lower availability of the DPA, thus a higher CO_2/DPA ratio, a computational investigation has been carried out starting from adduct **4** of Fig. 6 upon the removal of one, firstly, and later two DPA molecule(s). In particular, DPA molecule featuring N4 center, the less stabilizing amine in view of the long N4—H4 distance, was initially removed and the adduct optimized. The removal of one DPA molecule allows the isolation of both ionic pair **5** and **6**, the latter featuring a carbamic acid moiety stabilized by hydrogen bonding with two DPA molecules. The adducts **5** and **6**, shown in Fig. 8, are very close in energy, with a free energy difference being less than 1 kcal mol^{-1} in favor of adduct **5**. To gain a detailed analysis of the energetic feature of the **5**/**6** interconversion, the relaxed scan associated to the H3 proton transfer between N3 nitrogen and O2 oxygen revealed a barrierless process. The computational results highlight that already at a CO_2/DPA ratio of 0.333 both the ionic pair and the carbamic acid should be present in solution. It is also clear that the number of available hydrogen bond species in

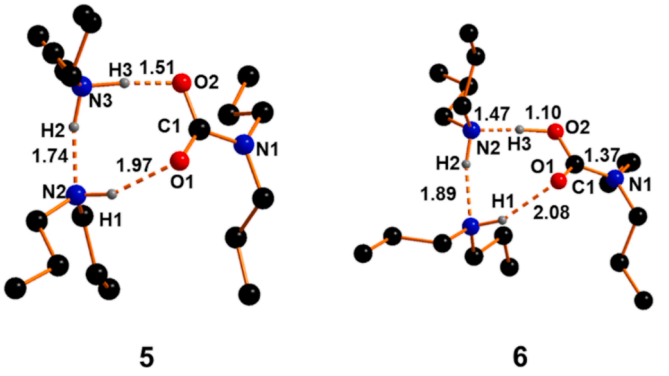

Fig. 8. Optimized structure of the adducts **5** (ionic pair stabilized by a DPA molecule) and **6** (carbamic acid stabilized by two DPA molecules). For the sake of clarity only the protons involved in H-bonding interactions have been shown.

solution influences the ratio between carbamate and carbamic acid.

By further increasing the CO_2 loading, it is plausible that some adducts **5** or also **6** can lose a DPA molecule for the activation of further CO_2. The free energy cost for the DPA removal is + 0.7 and + 1.6 kcal mol^{-1} starting from 5 and 6, respectively. In this regard, DFT analysis revealed that invariably starting from **5** or **6**, the only possible product is adduct **7**, shown in Fig. 9, featuring a hydrogen bonding interaction between a carbamic acid and a DPA molecule. In this condition, the most probable adduct for the activation of the newly incoming CO_2 could be **1**, shown in Fig. 3, featuring a CO_2/DPA ratio of 0.5. Starting from **1**, the computational analysis revealed that as the N2—H1 distance is gradually shortened, the system evolves through a Transition State $\mathbf{TS_{1\text{-}7}}$, shown in Fig. 9. In $\mathbf{TS_{1\text{-}7}}$, the H1 proton transfer from N1 to N2 is complete but the second proton H2 on N2 is immediately transferred to O1 with the formation of carbamic acid. In particular, the O1—H2 distance, 1.45 Å, appears particularly shortened from the starting value of 2.58 Å while the corresponding N2-–H2 is elongated up to 1.13 Å. The Transition State features a six-membered cycle with a *quasi*-formed N1-C1 distance, 1.51 Å. The nature of the TS has been confirmed by the detection of a single imaginary frequency at −35 cm^{-1}, associated with the combined proton transfers between N1 → N2 and N2 → O1. The estimated free energy barrier for the achievement of the $\mathbf{TS_{1\text{-}7}}$ is 11.7 kcal mol^{-1}, after which the system gains −14.9 kcal mol^{-1} for the achievement of adduct **7**, in Fig. 9.

The obtained carbamic acid in **7** could behave as a stabilizing agent toward the ionic pair in place of a DPA molecule with the formation of adduct like **8**, shown in Fig. 10. The IR reveals the appearance of a peak at 1654 cm^{-1} reasonably assigned to the carboxylic group of the carbamic acid. As the concentration of carbamic acid increases, another kind of adduct (**9**) is plausible in solution, featuring two carbamic acid moieties interacting through two strong hydrogen-bonds (Fig. 10). Interestingly, vibrational calculations have highlighted an IR peak at 2862 cm^{-1}, assigned to the *out-of-phase* O–H stretching of the cycle, in agreement with the experimental detection of a broad band in 2600–3100 cm^{-1} [25]. The formation of the adduct in Fig. 10 may explain the experimental NMR shift of the acid proton at higher ppm.

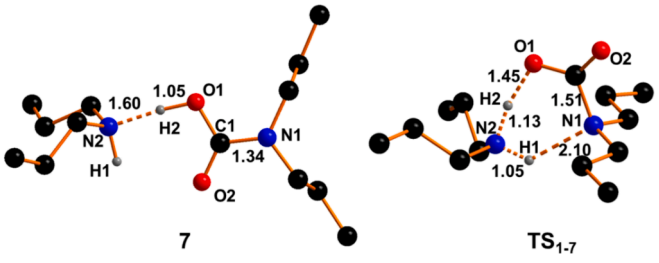

Fig. 9. Optimized structure of: adduct **7** and the Transition State $\mathbf{TS_{1\text{-}7}}$.

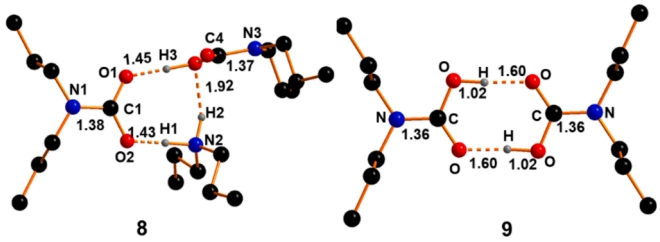

Fig. 10. Optimized structure of adducts **8** and **9**.

The formation of adduct **9** from two adducts **7** through the removal of two DPA molecules has been estimated to be exergonic by −5.7 kcal mol^{-1}. A complete schematic free energy profile for the obtainment of adduct **9** starting from **1** is shown in Fig. 11.

4. Conclusions

A detailed picture of the formation and the evolution of the products forming during the CO_2 absorption by DPA amines has been provided in relation with the CO_2/DPA ratio revealing a dynamic behavior. A representation of the main products at low as well as high CO_2 loadings is shown in Scheme 3. A small CO_2/DPA ratio favors the formation of the ionic pair carbamate/ammonium stabilized by DPA molecules without the formation of carbamic acid as hypothesized in Scheme 1. By increasing the CO_2/DPA ratio, the carbamic acid becomes predominant with the formation of some adducts based on it. The availability of hydrogen bond donors and acceptor from free DPA seem to be particularly fundamental for determining the most stable product, thus the ratio between carbamate and carbamic acid. Experimental investigations have confirmed the presence of carbamic acid only at high CO_2 loading with detection of a proton signal in the 10–12 ppm range. The experimental observations are confirmed by detailed DFT analysis which also provides a reasonable energetic pathway for the formation and the interconversion between the different species.

This manuscript represents a detailed study of the energetic/electronic features ruling the selective CO_2 absorption by solvent-free liquid amines and the obtained results could be particularly useful in the design of similar sorbents for energy efficient CO_2 capture processes. The rationalization of the water-free CO_2 absorption mechanism will be particularly significant in the perspective of formulating highly efficient amine-based sorbents in organic diluents. In particular, the presence of a diluent in the reaction environment should cause drastic effects on the most probable products of the CO_2 process. For example, the employment of a H-bonding donor solvent, such as glycolic species, may strongly stabilize the carbamate/ammonium ionic pair bypassing the formation of the carbamic acid, even as an intermediate of the reaction. In this perspective, some solvent or diluent molecules have to be

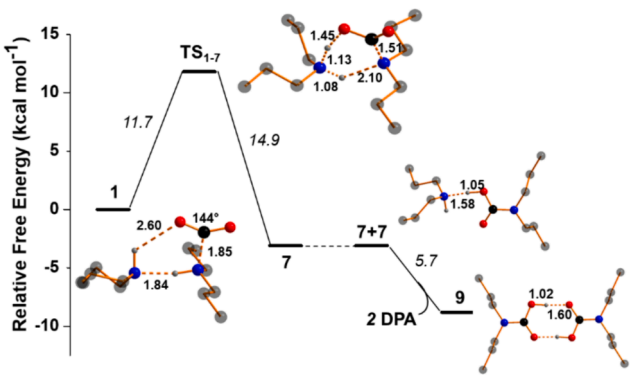

Fig. 11. Free Energy pathway (kcal/mol) for the achievement of adduct **9** from **1**.

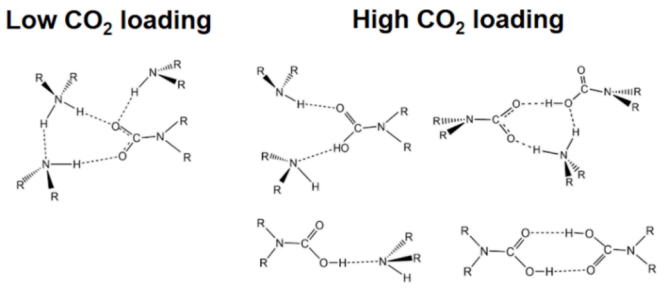

Scheme 3. Main products of the CO_2 absorption by DPA at low (left side) and high (right side) of CO_2 loadings.

considered explicitly in computational investigation. The deep knowledge of the products or reaction intermediates of CO_2 absorption will be a step beyond the design of effective acidic solid catalysts to lower the energy requirements associated with the CO_2 desorption step and sorbent regeneration.

CRediT authorship contribution statement

Gabriele Manca: Writing – review & editing, Writing – original draft, Investigation, Conceptualization. **Francesco Barzagli:** Writing – review & editing, Writing – original draft, Investigation, Conceptualization. **Jakub Nagy:** Methodology, Investigation. **Markéta Munzarová:** Methodology, Funding acquisition. **Maurizio Peruzzini:** Supervision. **Andrea Ienco:** Funding acquisition, Conceptualization.

Declaration of competing interest

The authors declare that they have no known competing financial interests or personal relationships that could have appeared to influence the work reported in this paper.

Data availability

No data was used for the research described in the article.

Acknowledgements

We acknowledge the CINECA award under the ISCRA initiative, for the availability of high-performance computing resources and support.

Appendix A. Supplementary data

Supplementary data to this article can be found online at https://doi.org/10.1016/j.fuel.2024.132859.

References

[1] M. Pathak, R. Slade, P.R. Shukla, J. Skea, R. Pichs-Madruga, D. Ürge-Vorsatz, Technical Summary. In: Climate Change 2022: Mitigation of Climate Change. Contribution of Working Group III to the Sixth Assessment Report of the Intergovernmental Panel on Climate Change, Technical Summary. In: Climate Change 2022: Mitigation of Climate Change. Contribution of Working Group III to the Sixth Assessment Report of the Intergovernmental Panel on Climate Change, in: Cambridge Univ. Press, Cambridge, UK and New York, NY, USA, 2022: pp. 51–147. Doi: 10.1017/9781009157926.002.

[2] Unfccc. United Nations Framework Convention on ClimateChange, The Glasgow Climate Pact –. Key Outcomes from COP26 2021. https://unfccc.int/process-and-meetings/the-paris-agreement/the-glasgow-climate-pact-key-outcomes-from-cop26.

[3] Singto S, Supap T, Idem R, Tontiwachwuthikul P, Tantayanon S, Al-Marri MJ, et al. Synthesis of new amines for enhanced carbon dioxide (CO2) capture performance: The effect of chemical structure on equilibrium solubility, cyclic capacity, kinetics of absorption and regeneration, and heats of absorption and regeneration. Sep Purif Technol 2016;167:97–107. https://doi.org/10.1016/j.seppur.2016.05.002.

[4] El Hadri N, Quang DV, Goetheer ELV, Abu Zahra MRM. Aqueous amine solution characterization for post-combustion CO2 capture process. Appl Energy 185 2017: 1433–49. https://doi.org/10.1016/j.apenergy.2016.03.043.

[5] Reynolds AJ, Verheyen TV, Adeloju SB, Meuleman E, Feron P. Towards Commercial Scale Postcombustion Capture of CO2 with Monoethanolamine Solvent: Key Considerations for Solvent Management and Environmental Impacts. Environ Sci Technol 2012;46:3643–54. https://doi.org/10.1021/es204051s.

[6] Zhang R, Zhang X, Yang Q, Yu H, Liang Z, Luo X. Analysis of the reduction of energy cost by using MEA-MDEA-PZ solvent for post-combustion carbon dioxide capture (PCC). Appl Energy 2017;205:1002–11. https://doi.org/10.1016/j.apenergy.2017.08.130.

[7] Zhang X, Zhang X, Liu H, Li W, Xiao M, Gao H, et al. Reduction of energy requirement of CO2 desorption from a rich CO2-loaded MEA solution by using solid acid catalysts. Appl Energy 2017;202:673–84. https://doi.org/10.1016/j.apenergy.2017.05.135.

[8] Zhang R, Li T, Zhang Y, Ha J, Xiao Y, Li C, et al. CuO modified KIT-6 as a high-efficiency catalyst for energy-efficient amine solvent regeneration. Sep Purif Technol 2022;300:121702. https://doi.org/10.1016/j.seppur.2022.121702.

[9] Zheng Y, Gao L, He S. Analysis of the mechanism of energy consumption for CO2 capture in a power system. Energy 2023;262:125103. https://doi.org/10.1016/j.energy.2022.125103.

[10] Zhang S, Shen Y, Zheng C, Xu Q, Sun Y, Huang M, et al. Recent advances, challenges, and perspectives on carbon capture. Front Environ Sci Eng 2024;18:75. https://doi.org/10.1007/s11783-024-1835-0.

[11] Shao P, Ye J, Shen Y, Zhang S, Zhao J. Recent advancements in carbonic anhydrase for CO2 capture: A mini review. Gas Sci Eng 2024;123:205237. https://doi.org/10.1016/j.jgsce.2024.205237.

[12] Alkhatib III, Galindo A, Vega LF. Systematic study of the effect of the co-solvent on the performance of amine-based solvents for CO2 capture. Sep Purif Technol 2022; 282:120093. https://doi.org/10.1016/j.seppur.2021.120093.

[13] Kollias L, Zhang D, Allec SI, Nguyen M-T, Lee M-S, Cantu DC, et al. Advanced Theory and Simulation to Guide the Development of CO2 Capture Solvents. ACS Omega 2022;7:12453–66. https://doi.org/10.1021/acsomega.1c07398.

[14] Wanderley RR, Pinto DDD, Knuutila HK. From hybrid solvents to water-lean solvents – A critical and historical review. Sep Purif Technol 2021;260:118193. https://doi.org/10.1016/j.seppur.2020.118193.

[15] Heldebrant DJ, Koech PK, Glezakou VA, Rousseau R, Malhotra D, Cantu DC. Water-Lean Solvents for Post-Combustion CO2 Capture: Fundamentals, Uncertainties, Opportunities, and Outlook. Chem Rev 2017;117:9594–624. https://doi.org/10.1021/acs.chemrev.6b00768.

[16] Karlsson HK, Makhool H, Karlsson M, Svensson H. Chemical absorption of carbon dioxide in non-aqueous systems using the amine 2-amino-2-methyl-1-propanol in dimethyl sulfoxide and N-methyl-2-pyrrolidone. Sep Purif Technol 2021;256: 117789. https://doi.org/10.1016/j.seppur.2020.117789.

[17] Karlsson HK, Sanku MG, Svensson H. Absorption of carbon dioxide in mixtures of N-methyl-2-pyrrolidone and 2-amino-2-methyl-1-propanol. Int J Greenh Gas Control 2020;95:102952. https://doi.org/10.1016/j.ijggc.2019.102952.

[18] Barzagli F, Bhatti UH, Kazmi WW, Peruzzini M. Solid acid catalysts for low-temperature regeneration of non-aqueous sorbents: An innovative technique for energy-efficient CO2 capture processes. Carbon Capture Sci Technol 2023;8: 100124. https://doi.org/10.1016/j.ccst.2023.100124.

[19] Hedayati A, Feyzi F. Towards water-insensitive CO2-binding organic liquids for CO2 absorption: Effect of amines as promoter. J Mol Liq 2020;306:112938. https://doi.org/10.1016/j.molliq.2020.112938.

[20] Zheng F, Heldebrant DJ, Mathias PM, Koech P, Bhakta M, Freeman CJ, et al. Bench-Scale Testing and Process Performance Projections of CO2 Capture by CO2 –Binding Organic Liquids (CO2 BOLs) with and without Polarity-Swing-Assisted Regeneration. Energy Fuel 2016;30:acs.energyfuels.5b02437. https://doi.org/10.1021/acs.energyfuels.5b02437.

[21] Wanderley RR, Yuan Y, Rochelle GT, Knuutila HK. CO2 solubility and mass transfer in water-lean solvents. Chem Eng Sci 2019;202:403–16. https://doi.org/10.1016/j.ces.2019.03.052.

[22] Yu Y, Shen Y, Zhou X, Liu F, Zhang S, Lu S, et al. Relationship between tertiary amine's physical property and biphasic solvent's CO2 absorption performance: Quantum calculation and experimental demonstration. Chem Eng J 2022;428: 131241. https://doi.org/10.1016/j.cej.2021.131241.

[23] Kortunov PV, Siskin M, Baugh LS, Calabro DC. In Situ Nuclear Magnetic Resonance Mechanistic Studies of Carbon Dioxide Reactions with Liquid Amines in Non-aqueous Systems: Evidence for the Formation of Carbamic Acids and Zwitterionic Species. Energy Fuel 2015;29:5940–66. https://doi.org/10.1021/acs.energyfuels.5b00985.

[24] Kortunov PV, Siskin M, Paccagnini M, Thomann H. CO2 Reaction Mechanisms with Hindered Alkanolamines: Control and Promotion of Reaction Pathways. Energy Fuel 2016;30:acs.energyfuels.5b02582. https://doi.org/10.1021/acs.energyfuels.5b02582.

[25] Barzagli F, Lai S, Mani F. A new class of single-component absorbents for reversible carbon dioxide capture under mild conditions. ChemSusChem 2015;8:184–91. https://doi.org/10.1002/cssc.201402421.

[26] Barzagli F, Mani F, Peruzzini M. A Comparative Study of the CO2 Absorption in Some Solvent-Free Alkanolamines and in Aqueous Monoethanolamine (MEA). Environ Sci Technol 2016;50:7239–46. https://doi.org/10.1021/acs.est.6b00150.

[27] Ma C, Pietrucci F, Andreoni W. CO2 Capture and Release in Amine Solutions: To What Extent Can Molecular Simulations Help Understand the Trends? Molecules 2023;28:6447. https://doi.org/10.3390/molecules28186447.

[28] Ma M, Liu Y, Chen Y, Jing G, Lv B, Zhou Z, et al. Regulatory mechanism of a novel non-aqueous absorbent for CO2 capture using 2-amino-2-methyl-1-propanol: Low

viscosity and energy efficient. J CO2 Util 2023;67:102277. https://doi.org/10.1016/j.jcou.2022.102277.
[29] Xiang J, Wei D, Mao W, Liu T, Luo Q, Huang Y, et al. Comprehensive kinetic study of carbon dioxide absorption in blended tertiary/secondary amine solutions: Experiments and simulations. Sep Purif Technol 2024;330:125310. https://doi.org/10.1016/j.seppur.2023.125310.
[30] Matsuzaki Y, Yamada H, Chowdhury FA, Yamamoto S, Goto K. Ab Initio Study of CO2 Capture Mechanisms in Aqueous 2-Amino-2-methyl-1-propanol: Electronic and Steric Effects of Methyl Substituents on the Stability of Carbamate. Ind & Eng Chem Res 2019;58:3549–54. https://doi.org/10.1021/acs.iecr.8b06229.
[31] Ben Said R, Kolle JM, Essalah K, Tangour B, Sayari A. A Unified Approach to CO2 –Amine Reaction Mechanisms. ACS Omega 2020;5:26125–33. https://doi.org/10.1021/acsomega.0c03727.
[32] Wang R, Liu S, Li Q, Zhang S, Wang L, An S. CO2 capture performance and mechanism of blended amine solvents regulated by N-methylcyclohexyamine. Energy 2021;215:119209. https://doi.org/10.1016/J.ENERGY.2020.119209.
[33] Cantu DC, Malhotra D, Nguyen M, Koech PK, Zhang D, Glezakou V, et al. Molecular-Level Overhaul of γ-Aminopropyl Aminosilicone/Triethylene Glycol Post-Combustion CO2 -Capture Solvents. ChemSusChem 2020;13:3429–38. https://doi.org/10.1002/cssc.202000724.
[34] Malhotra D, Cantu DC, Koech PK, Heldebrant DJ, Karkamkar A, Zheng F, et al. Directed Hydrogen Bond Placement: Low Viscosity Amine Solvents for CO2 Capture. ACS Sustain Chem Eng 2019;7:7535–42. https://doi.org/10.1021/acssuschemeng.8b05481.
[35] Barzagli F, Giorgi C, Mani F, Peruzzini M. Reversible carbon dioxide capture by aqueous and non-aqueous amine-based absorbents: A comparative analysis carried out by 13C NMR spectroscopy. Appl Energy 2018;220:208–19. https://doi.org/10.1016/j.apenergy.2018.03.076.
[36] Hu XE, Yu Q, Barzagli F, Li C, Fan M, Gasem KAM, et al. NMR Techniques and Prediction Models for the Analysis of Species Formed in CO2 Capture Processes with Amine-Based Sorbents: A Critical Review. ACS Sustain Chem Eng 2020;8:6173–93. https://doi.org/10.1021/acssuschemeng.9b07823.
[37] Bhatti UH, Ienco A, Peruzzini M, Barzagli F. Unraveling the Role of Metal Oxide Catalysts in the CO2 Desorption Process from Nonaqueous Sorbents: An Experimental Study Carried out with 13C NMR. ACS Sustain Chem Eng 2021;9:15419–26. https://doi.org/10.1021/acssuschemeng.1c04026.
[38] Barzagli F, Lai S, Mani F. CO2 Capture by Liquid Solvents and their Regeneration by Thermal Decomposition of the Solid Carbonated Derivatives. Chem Eng Technol 2013;36:1847–52. https://doi.org/10.1002/ceat.201300225.
[39] Chen G, Chen G, Peruzzini M, Barzagli F, Zhang R. Investigating the Performance of Ethanolamine and Benzylamine Blends as Promising Sorbents for Postcombustion CO2 Capture through 13C NMR Speciation and Heat of CO2 Absorption Analysis. Energy Fuel 2022;36:9203–12. https://doi.org/10.1021/acs.energyfuels.2c01930.
[40] Grimme S. Semiempirical hybrid density functional with perturbative second-order correlation. J Chem Phys 2006;124:34108. https://doi.org/10.1063/1.2148954.
[41] M.J. Frisch, G.W. Trucks, H.B. Schlegel, G.E. Scuseria, M. a. Robb, J.R. Cheeseman, G. Scalmani, V. Barone, G. a. Petersson, H. Nakatsuji, X. Li, M. Caricato, a. V. Marenich, J. Bloino, B.G. Janesko, R. Gomperts, B. Mennucci, H.P. Hratchian, J. V. Ortiz, a. F. Izmaylov, J.L. Sonnenberg, Williams, F. Ding, F. Lipparini, F. Egidi, J. Goings, B. Peng, A. Petrone, T. Henderson, D. Ranasinghe, V.G. Zakrzewski, J. Gao, N. Rega, G. Zheng, W. Liang, M. Hada, M. Ehara, K. Toyota, R. Fukuda, J. Hasegawa, M. Ishida, T. Nakajima, Y. Honda, O. Kitao, H. Nakai, T. Vreven, K. Throssell, J. a. Montgomery Jr., J.E. Peralta, F. Ogliaro, M.J. Bearpark, J.J. Heyd, E.N. Brothers, K.N. Kudin, V.N. Staroverov, T. a. Keith, R. Kobayashi, J. Normand, K. Raghavachari, a. P. Rendell, J.C. Burant, S.S. Iyengar, J. Tomasi, M. Cossi, J.M. Millam, M. Klene, C. Adamo, R. Cammi, J.W. Ochterski, R.L. Martin, K. Morokuma, O. Farkas, J.B. Foresman, D.J. Fox, G16_C01, (2016) Gaussian 16, Revision C.01, Gaussian, Inc., Wallin.
[42] Barone V, Cossi M. Quantum Calculation of Molecular Energies and Energy Gradients in Solution by a Conductor Solvent Model. J Phys Chem A 1998;102:1995–2001. https://doi.org/10.1021/jp9716997.
[43] Schäfer A, Huber C, Ahlrichs R. Fully optimized contracted Gaussian basis sets of triple zeta valence quality for atoms Li to Kr. J Chem Phys 1994;100:5829–35. https://doi.org/10.1063/1.467146.
[44] Switzer JR, Ethier AL, Flack KM, Biddinger EJ, Gelbaum L, Pollet P, et al. Reversible Ionic Liquid Stabilized Carbamic Acids: A Pathway Toward Enhanced CO2 Capture. Ind Eng Chem Res 2013;52:13159–63. https://doi.org/10.1021/ie4018836.
[45] Liu A-H, Ma G-T, Ren B-H, Zhang J-Y, Lu X-B. Alkoxy-Functionalized Amines as Single-Component Water-Lean CO2 Absorbents with High Efficiency: The Benefit of Stabilized Carbamic Acid. Ind Eng Chem Res 2022;61:7080–9. https://doi.org/10.1021/acs.iecr.2c01361.
[46] Didas SA, Sakwa-Novak MA, Foo GS, Sievers C, Jones CW. Effect of Amine Surface Coverage on the Co-Adsorption of CO2 and Water: Spectral Deconvolution of Adsorbed Species. J Phys Chem Lett 2014;5:4194–200. https://doi.org/10.1021/jz502032c.
[47] Yu J, Chuang SSC. The Structure of Adsorbed Species on Immobilized Amines in CO2 Capture: An in Situ IR Study. Energy Fuel 2016;30:7579–87. https://doi.org/10.1021/acs.energyfuels.6b01423.
[48] Srikanth CS, Chuang SSC. Infrared Study of Strongly and Weakly Adsorbed CO2 on Fresh and Oxidatively Degraded Amine Sorbents. J Phys Chem C 2013;117:9196–205. https://doi.org/10.1021/jp311232f.
[49] Danon A, Stair PC, Weitz E. FTIR Study of CO2 Adsorption on Amine-Grafted SBA-15: Elucidation of Adsorbed Species. J Phys Chem C 2011;115:11540–9. https://doi.org/10.1021/jp200914v.
[50] Parks C, Alborzi E, Akram M, Pourkashanian M. DFT Studies on Thermal and Oxidative Degradation of Monoethanolamine. Ind & Eng Chem Res 2020;59:15214–25. https://doi.org/10.1021/acs.iecr.0c03003.
[51] Mulliken RS. Electronic Population Analysis on LCAO–MO Molecular Wave Functions. I. J Chem Phys 1955;23:1833–40. https://doi.org/10.1063/1.1740588.
[52] Mealli C, Hoffmann R, Stockis A. Molecular orbital analysis of the bonding capabilities of carbon disulfide and carbon dioxide toward transition metal fragments. Inorg Chem 2002;23:56–65. https://doi.org/10.1021/ic00169a014.
[53] Mondal B, Song J, Neese F, Ye S. Bio-inspired mechanistic insights into CO2 reduction. Curr Opin Chem Biol 2015;25:103–9. https://doi.org/10.1016/j.cbpa.2014.12.022.
[54] Álvarez A, Borges M, Corral-Pérez JJ, Olcina JG, Hu L, Cornu D, et al. CO2 Activation over Catalytic Surfaces. ChemPhysChem 2017;18:3135–41. https://doi.org/10.1002/cphc.201700782.
[55] Cavalleri M, Damiano C, Manca G, Gallo E. Protonated Porphyrins: Bifunctional Catalysts for the Metal-Free Synthesis of N -Alkyl-Oxazolidinones. Chem – A Eur J 2023;29:1–7. https://doi.org/10.1002/chem.202202729.
[56] Zhao Y, Han B, Liu Z. Ionic-Liquid-Catalyzed Approaches under Metal-Free Conditions. Acc Chem Res 2021;54:3172–90. https://doi.org/10.1021/acs.accounts.1c00251.
[57] Saptal VB, Bhanage BM. N-Heterocyclic Olefins as Robust Organocatalyst for the Chemical Conversion of Carbon Dioxide to Value-Added Chemicals. ChemSusChem 2016;9:1980–5. https://doi.org/10.1002/cssc.201600467.
[58] Liu A-H, Dang Y-L, Zhou H, Zhang J-J, Lu X-B. CO2 Adducts of Carbodicarbenes: Robust and Versatile Organocatalysts for Chemical Transformation of Carbon Dioxide into Heterocyclic Compounds. ChemCatChem 2018;10:2686–92. https://doi.org/10.1002/cctc.201800148.
[59] Sonzini P, Damiano C, Intrieri D, Manca G, Gallo E. A Metal-Free Synthesis of N -Aryl Oxazolidin-2-Ones by the One-Pot Reaction of Carbon Dioxide with N -Aryl Aziridines. Adv Synth Catal 2020;362:2961–9. https://doi.org/10.1002/adsc.202000175.